

Feedforward Quantum Control and Coherence Protection of Single Electron Spin in Diamond using Deep Learning

Nanyang Xu,^{1,*} Feifei Zhou,¹ Xiangyu Ye,² Xue Lin,¹ Bao Chen,¹
Ting Zhang,¹ Feng Yue,³ Bing Chen,¹ Ya Wang,^{2,†} and Jiangfeng Du^{2,‡}

¹*School of Physics, Hefei University of Technology, Hefei, Anhui 230009, China*

²*CAS Key Laboratory of Microscale Magnetic Resonance,*

University of Science and Technology of China, Hefei 230026, China

³*Engineering Research Center of Safety Critical Industrial Measurement
and Control Technology, Ministry of Education, Hefei 230009*

Measurement-based realtime control is an important strategy in quantum information processing, which is applied in fields from qubit readout to error corrections. However, the time cost of quantum measurement inevitably induces a latency in the control process and limits its performance. Here we introduce the deep learning approach to relax this restriction by predicting and compensating the latency-induced control error. We experimentally implement feedforward quantum control of a single-spin system of nitrogen-vacancy (NV) center in diamond to protect the coherence of the electron spin. The new approach enhances the decoherence time as well as the spectrum resolution of Ramsey interferometry about three times comparing with conventional scheme. This enables resolving optically indistinguishable NV centers from their magnetic spectrum with a frequency difference less than 20 kHz. A theoretical model is proposed to explain the improvement, where we show that the low-frequency magnetic noise is perfectly reduced. This scheme could be applied in general measurement schemes and extended to other quantum control systems.

INTRODUCTION

Protection of qubit coherence against noise is vital in quantum computation, quantum simulation and sensing. Many methods are proposed and implemented, including open-loop techniques such as optimal control [1, 2] and dynamical decoupling[3, 4], as well as close-loop approaches like the feedback control. Nevertheless, optimal control requires precise knowledge of the target system and cannot be applied universally. Dynamical decoupling approach, similar to a band-pass filter, removes all the signal outside the selected frequency band, and can only work with task that is commuted with the control operators, *e.g.*, sensing of alternative-current magnetic field or nuclear spins. In contrast to open-loop approaches, feedback control can be applied generally regardless of the system model. It has been used in magnetometry for sensing signals with fixed frequency[5, 6]. But for a general time-varying signal like the fluctuating noise, the quantum-measurement-induced latency between detection and responding is thus required to be within the correlation time of the signal[7–13]. To relax this restriction, an alternative strategy is to predict the trend of the noise in the subsequent period, and compensate the latency-induced error in advance. This strategy, known as the feedforward control, could enhance the performance of measurement-based quantum control in principle, especially in the cases when qubit readout is quite slow, but practical realization of this technique remains unclear.

Machine learning is a group of methods that are well developed in computer science and has been applied in quantum control fields including Hamilto-

nian learning[14], qubit readout[15–19] and experimental controls[20, 21]. Recently, the deep learning model (DL)[22] is emerging as a powerful tool, which can deal with complicated problems with multiple layers of artificial neural network such as the many-body problem[23]. Another potential application is to combine DL with quantum feedforward control by using its ability in time-series prediction[24], which has been applied in stock-price prediction and weather forecast.

Here we propose a deep-learning-assisted feedforward control scheme and show its advantage on a solid-state single spin associated with the nitrogen-vacancy (NV) center in diamond. In our scheme, the target spin works as a quantum sensor to detect the magnetic noise used to train the DL agent. The agent learns the noise model and predicts the forthcoming value in realtime and feeds this value to correct the corresponding error on the spin. Due to the low optical detection efficiency, there's an intrinsic latency in magnetic-noise readout process in the order of seconds. By using the new scheme, we demonstrate a feedforward Ramsey experiment and show a three-fold improvement in the line-width of its spectrum as well as the spin coherence time comparing with conventional scheme. As an application of this technique, we resolve an NV pair with a difference less than 20 kHz in resonance spectrum, enabling the possibility to use aligned NV pair as a quantum register in the future.

RESULTS

NV center in diamond has been developed as a multi-function sensor for magnetic field[25–30], electric

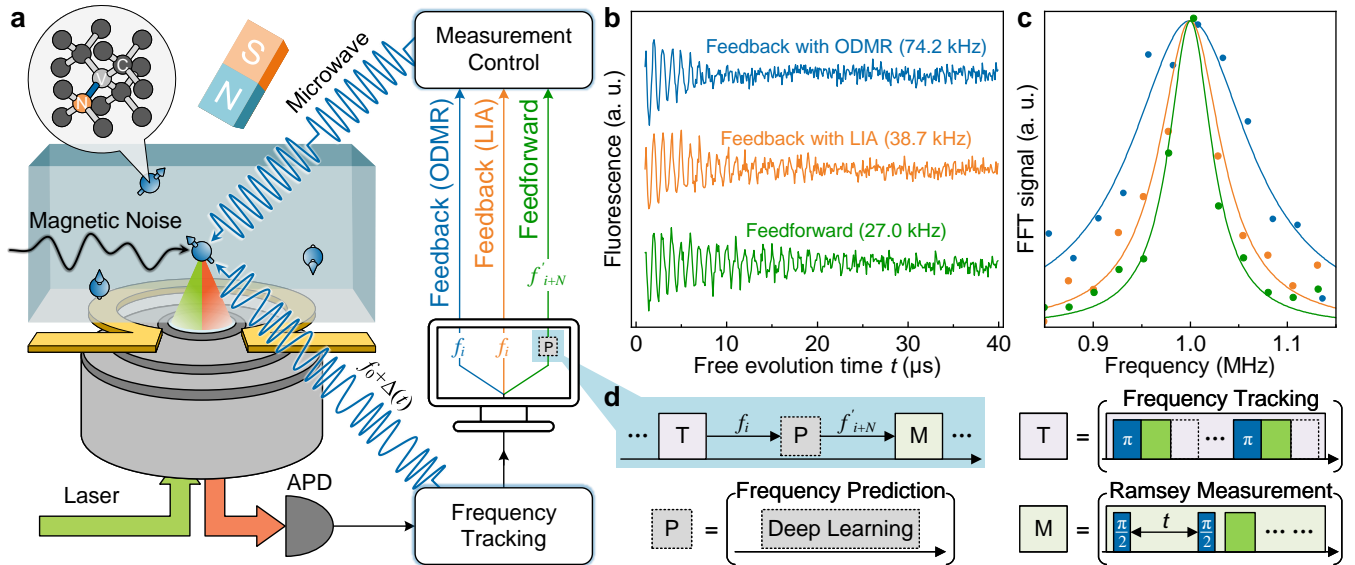


FIG. 1. (Color online) **General scheme of measurement-based close-loop quantum control.** **a)** Schematic of the control scheme and experiment setup. A frequency tracking process tracks the resonance frequency f_i of electron spin using LIA or ODMR method at each time step i , where the microwave frequency is swept in the adjacent range Δ of an initial frequency f_0 and the emitting fluorescence is acquired via the avalanche photodiode (APD) accordingly. A control computer reads the detected value and feeds the detected (predicted) frequency to the measurement controller for the subsequent experiment loops. We realize three kinds of experiment schemes: feedback with ODMR (blue arrow), feedback with LIA (orange arrow), and feedforward (green arrow), respectively. **b-c)** Experiment results (b) and their FFT spectra (c) of Ramsey measurement with a bias of 1 MHz off the resonance using the three specific experiment schemes in (a). The bracketed frequency in (b) is the corresponding line-width of the FFT spectrum. **d)** Detailed control sequence of the experiment schemes. The notation \mathbf{T} represents pulse sequence of frequency detection and \mathbf{M} is general-purpose measurement, where Ramsey measurement is used in our experiment and t is the free evolution time. The period of frequency tracking is defined as τ , which includes the time cost of frequency detection and Ramsey measurements. Label \mathbf{P} denotes deep learning agent that predicts the future values f'_i based on history detections and is only used in the feedforward scheme.

field[31, 32] and temperature[33, 34], as well as the nano-scale magnetic resonances [35–39]. Besides, it also works as quantum resources[40–43] for computation[44–48], simulation[49, 50] and network[51–55]. Because of the high gyro-magnetic ratio, electron spin in NV center is quite sensitive and often suffers from low-frequency magnetic noise arising from mechanical vibrations or temperature changes, resulting in broadening of resonance lines and spin decoherence. We consider three measurement-based schemes (Fig.1A) to solve this problem and use the Ramsey measurement as an application, where the magnetic noise is obtained by tracking the electron-spin resonant frequency and compensated immediately. The first one is feedback control using conventional method without prediction. The frequency is detected by finding the peak of the optically-detected magnetic resonance (ODMR) spectrum, which usually requires scanning a wide range of microwave (MW) frequencies for a successful fitting. The result of this scheme is shown in the upper plot of Fig.1B.

In the second and third schemes, we adopt the lock-in amplifier (LIA) method to improve the efficiency of frequency detection[56]. Unlike ODMR, LIA gets the resonant frequency directly by a hardware synchronization

of photon counts and MW frequencies via an external oscillating reference. It scans only a small range near the resonant frequency, thus enables us updating the detection in realtime and tracking the magnetic noise continuously. The second scheme also uses the feedback strategy and the result is shown in the middle plot of Fig.1B, which has a two-fold improvement in the Ramsey measurement comparing with that using ODMR method.

Because of low photon counts of single-spin system, LIA use a detection window around 20 s in experiment to achieve a high signal-noise ratio (SNR). This latency fundamentally limits the efficiency of feedback control. In the third scheme, feedforward strategy is utilized to further improve the performance assisted with the deep-learning method. The feedforward strategy, different from feedback control that uses detected value directly, predicts the trend of noise in the future and use the forthcoming value instead to correct the error. The result is shown in the lower plot of Fig.1B, where the performance is about three-fold improved comparing with the conventional scheme. We further plot the fitted line-width (*i.e.*, the full width of the peak at half its maximum, proportional to inverse of the coherence time T_2^*) of the FFT spectrum in Fig.1C to show the mentioned improvements

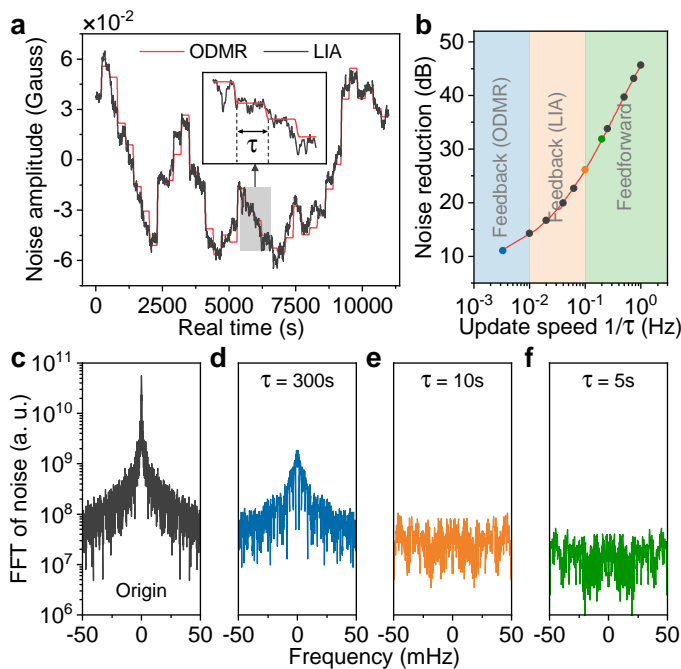


FIG. 2. (Color online) **Analysis of magnetic noise reduction.** **a)** Tracking of magnetic noise using both ODMR (red line) and LIA (black line) methods. The update period τ of ODMR (LIA) method is fixed at 300 (1) s specifically. **b)** Noise reduction efficiency in an ideal feedback control (with no detection delay) using different update speeds $1/\tau$, which is obtained from numerical simulations based on the detected noise in (a). The filled areas in different colors represent the update speeds that can be realized in the specific control schemes, *i.e.*, ODMR-based (blue) and LIA-based feedback (orange), as well as feedforward (green). **c-f)** FFT spectrum of the noise before (c) and after (d-f) feedback control, where (d-f) associate with the update speed 0.0033, 0.1, and 0.2 Hz in (b), respectively.

directly. Note that, all the schemes are realized using a uniform control sequence in Fig.1D for comparison.

To understand this improvement, we first numerically calculate the FFT spectrum of noise after time-delayed correction depending on different update periods τ . Fig.2A(C) shows the experimentally-observed magnetic noise (FFT transform of the noise) via LIA detection. The updated period τ in the three experiment schemes refers to 300 s, 10 s and 5 s specifically, and the corresponding spectra after correction are shown in Fig.2D-F. One can find that the shorter the time delay is, the better the noise can be corrected (Fig.2B), which highlights the role of detection delay in measurement-based quantum control. Noted that the latency of the feedback control, which is about half the window (*i.e.*, 10 s for $\tau = 20$ s). The equivalent update period of 5 s in the feedforward scheme is taken into account the prediction of the noise in advance of 5 seconds (Fig.3D).

In the feedforward scheme, we adopt the long short-

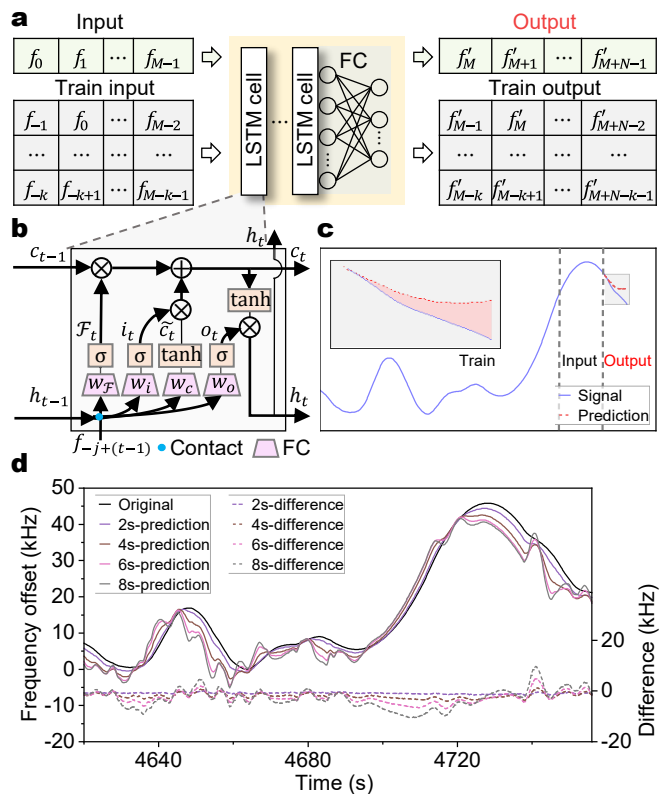


FIG. 3. (Color online) **Noise Prediction using deep learning.** **a)** Architecture of the model. The DL agent consists of basic LSTM cells followed by a fully-connected (FC) network used to bridge layers with different dimensions. It uses recent M values of f_t as input and generates N predicted values of f'_t . The history data for training is divided into k sequences, each of which is shifted forward one value for each step. **b)** Schematic of a basic LSTM cell. h_t (c_t) is the output (memory state) of the cell at time step t . $j = 0, 1, \dots, k$ is the index of the sequence. \oplus , \otimes , σ and \tanh are pointwise addition, pointwise multiplication, sigmoid activation and hyperbolic tangent activation, respectively. The operation **contact** is to generate a tuple consisted of the two inputs. **c)** The data diagram in noise prediction. The inset plot highlights the difference between original and predicted signals. **d)** The comparison and difference (the secondary y axis) between original and predicted noise with different prediction lengths N .

term memory (LSTM)[57], *i.e.*, an improved version of the recurrent neural network (RNN) for noise prediction. In Fig.3A, our model consists of basic LSTM cells cascading in a chain and a fully-connected (FC) network layer. As shown in Fig.3B, each basic LSTM cell get the output h_{t-1} of the previous cell and current frequency $f_{-j+(t-1)}$ together as input, then it calculate four inner vectors (i_t , F_t , \tilde{c}_t and o_t) each by a sub-network of a FC and an activation function to generate the memory state c_t and final output h_t of the cell. The memory state c_t maintains all the information of the cell. In every time step, forget gate F_t controls how much old information remains in the cell,

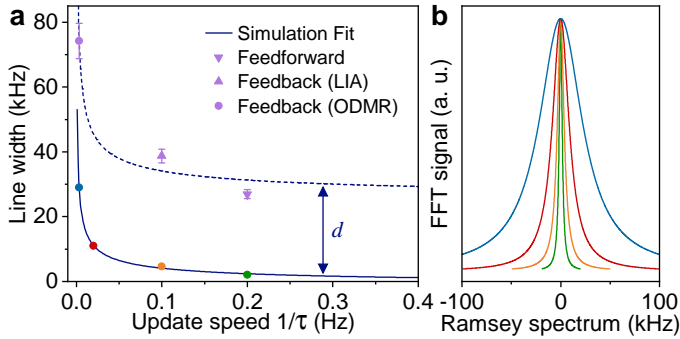


FIG. 4. (Color online) **Performance of noise reduction with Ramsey measurement.** **a)** The dependence of Ramsey line-width on the update speeds. The dots fitted by the solid line are obtained from numerical simulation based on the detected noise in Fig.2A. The shapes fitted by the dashed line are the line-widths from experimental results in Fig.1C. The simulation and experimental results are fitted using the same mathematical function except for a residual line-width d . **b)** FFT spectra of the simulation results using Ramsey measurements in (a).

and input gate i_t determines how much new information is introduced. The value generated in the current cell is set to output gate o_t . The weight matrices ($W_{\mathcal{F}}$, W_i , W_c and W_o) of these sub-networks are obtained by training the network with given input and output from history data.

The work flow of the noise prediction is shown in Fig.3C. In prior, history data recorded from LIA is fed to the agent to train the neural network. In experiment, the agent gets recent detected values of M seconds as input and predicts N -second values as output, where N (M) is the prediction (sequence) length. We further compare original and predicted signals directly as well as their difference in Fig.3D with different prediction lengths N . The difference is shown to become larger and larger with N increasing. This fact indicates a trade-off between the fidelity and prediction length N to compensate the detection delay. For example, in our experiment the best noise reduction performance is achieved when N is about 5 s, while the detection delay is 10 s.

To evaluate the performance of noise reduction, we simulate the Ramsey measurements and analyze the broadening of line-width when the noise in Fig.2A is applied[56]. For different update speeds $v = 1/\tau$, the fitted line-width l is show in Fig.4A with the corresponding spectrum in Fig.4B, where a relation $l = 1/v^n$ is used to fit the data (the solid line). One can find that, this scheme can remove almost all the noise if the update speed exceeds the noise frequency. The experimental result matches well with this relation (the dashed line) except for a residual broadening (*i.e.*, $l = 1/v^n + d$). This broadening $d \sim 26$ kHz comes from noises due to the high-frequency part outside the frequency range in Fig.2C, such as the intrinsic spin-bath-induced noise.

Ramsey measurement has a wide range of applications in magnetic resonance (MR) sciences and sensing. Here as an example, we apply this method for a high-resolution spectroscopy of NV centers. As shown in Fig.5C, our method resolves two resonant peaks with a splitting less than 20 kHz, which is not visible in conventional experiments even when the ODMR-based feedback strategy is used (Fig.5A). Because nuclear spin is not observed in the corresponding dynamical decoupling spectroscopy [56], we deduce that this spectrum comes from an NV pair (NV2) with two centers aligned in the same direction. The tiny difference in resonate frequency is possibly because of electron-spin zero-field splitting. This method can be used to address individual NV centers of aligned NV pair by MR spectroscopy in the future.

The experiment is performed using a single Nitrogen-Vacancy (NV) center in a ^{12}C -purified single-crystal diamond. As shown in Fig.1A, the NV center is addressed by a home-built confocal microscope system. A 532-nm green laser passes through a 100X objective and is focused on the center. The fluorescence is emitted through the same objective and collected by an APD. The output signal of APD is detected by a time tagger for a general-purpose measurement and a mixed-signal data acquisition system for LIA frequency tracking. A static magnetic field around 50 mT is applied along the NV axis to split the sub-levels and the associated nitrogen nuclear spin is polarized as well. There are double microwave systems in the setup. The first one (Rohde&Schwarz SMIQ03B) is used to manipulate the electron-spin state for general purpose measurements. The other one (Rigol DSG3065B) outputs frequency-modulation microwave that is used for the LIA detection. These two microwave systems are bridged together and amplified by an amplifier (Mini-Circuits ZHL-42W). An impedance-matched copper slot line with an Ω -type ring is used to radiate the micro-wave fields. All the electronic and microwave devices are synchronized by a 10-MHz atomic clock source.

CONCLUSION

To conclude, we propose and implement a novel feed-forward quantum control scheme by learning the knowledge of low-frequency noise and correct the corresponding error in real-time. The result shows almost all the detectable noise can be reduced in experiment. There're two ways to further improve the performance. The first way is to enhance the spin-state readout efficiency and thus the detection speed is increased and the corresponding frequency range of detectable noise is enlarged. The second way is to optimize the performance of prediction, *i.e.*, trying more complicated deep-learning models and providing more computational resources for training and processing. Comparing with coherent feedback scheme

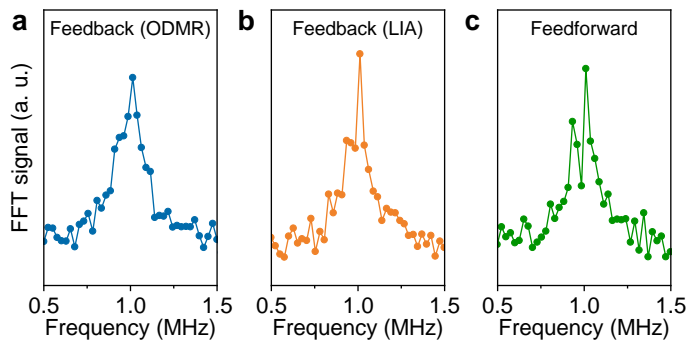


FIG. 5. (Color online) **Application of feedforward Ramsey measurements.** a-c) FFT spectrum corresponding to the Ramsey measurement of an NV pair using (a) ODMR-based feedback, (b) LIA-based feedback and (c) feedforward schemes.

that often uses nuclear spins as ancillary qubits[58] or quantum memory[59], our scheme requires no extra quantum resources and can work with general-purpose measurements. This approach can find applications in spin-based quantum computation, quantum simulation and nano-scale sensing (*e.g.*, magnetic fields, temperature or electric fields), and be easily extended to other quantum systems.

ACKNOWLEDGEMENT

This work was supported by the National Key R&D Program of China (Grants No. 2018YFA0306600, 2017YFA0305000 and 2020YFA0309400), the National Natural Science Foundation of China (Grants No. 81788101, 11775209 and 12174081), the CAS (Grants No. XDC07000000, GJJSTD20200001 and QYZDYSSW-SLH004), the Anhui Initiative in Quantum Information Technologies (Grant No. AHY050000), the Fundamental Research Funds for the Central Universities. The computational library Qutip [60] is used in numerical simulations and the data plots are generated using the graphics environment Matplotlib[61]. The deep learning model is implemented using the machine learning framework PyTorch[62].

* nyxu@hfut.edu.cn

† ywustc@ustc.edu.cn

‡ djf@ustc.edu.cn

- [1] G. Waldherr, Y. Wang, S. Zaiser, M. Jamali, T. Schulte-Herbrüggen, H. Abe, T. Ohshima, J. Isoya, J. F. Du, P. Neumann, and J. Wrachtrup, *Nature* **506**, 204 (2014).
- [2] F. Dolde, V. Bergholm, Y. Wang, I. Jakobi, B. Naydenov, S. Pezzagna, J. Meijer, F. Jelezko, P. Neumann, T. Schulte-Herbrüggen, J. Biamonte, and J. Wrachtrup, *Nature communications* **5**, 3371 (2014).

- [3] J. Du, X. Rong, N. Zhao, Y. Wang, J. Yang, and R. Liu, *Nature* **461**, 1265 (2009).
- [4] G. De Lange, Z. Wang, D. Riste, V. Dobrovitski, and R. Hanson, *Science* **330**, 60 (2010).
- [5] C. Bonato, M. S. Blok, H. T. Dinani, D. W. Berry, M. L. Markham, D. J. Twitchen, and R. Hanson, *Nature nanotechnology* **11**, 247 (2016).
- [6] R. Santagati, A. Gentile, S. Knauer, S. Schmitt, S. Paesani, C. Granade, N. Wiebe, C. Osterkamp, L. McGuinness, J. Wang, M. Thompson, J. Rarity, F. Jelezko, and A. Laing, *Physical Review X* **9**, 021019 (2019).
- [7] D. Rist, C. C. Bultink, K. W. Lehnert, and L. DiCarlo, *Physical Review Letters* **109**, 240502 (2012).
- [8] D. Rist, M. Dukalski, C. A. Watson, G. de Lange, M. J. Tiggelman, Y. M. Blanter, K. W. Lehnert, R. N. Schouten, and L. DiCarlo, *Nature* **502**, 350 (2013).
- [9] J. Cramer, N. Kalb, M. A. Rol, B. Hensen, M. S. Blok, M. Markham, D. J. Twitchen, R. Hanson, and T. H. Taminiau, *Nature Communications* **7**, 11526 (2016).
- [10] K. C. Cox, G. P. Greve, J. M. Weiner, and J. K. Thompson, *Physical Review Letters* **116**, 093602 (2016).
- [11] P. Campagne-Ibarcq, S. Jezouin, N. Cottet, P. Six, L. Bretheau, F. Mallet, A. Sarlette, P. Rouchon, and B. Huard, *Physical Review Letters* **117**, 060502 (2016).
- [12] H. Bluhm, S. Foletti, D. Mahalu, V. Umansky, and A. Yacoby, *Physical Review Letters* **105**, 216803 (2010).
- [13] T. Nakajima, Y. Kojima, Y. Uehara, A. Noiri, K. Takeda, T. Kobayashi, and S. Tarucha, *Physical Review Applied* **15**, L031003 (2021).
- [14] J. Wang, S. Paesani, R. Santagati, S. Knauer, A. A. Gentile, N. Wiebe, M. Petruzzella, J. L. O'Brien, J. G. Rarity, and A. Laing, *Nature Physics* **13**, 551 (2017).
- [15] E. Magesan, J. M. Gambetta, A. D. Crcoles, and J. M. Chow, *Physical review letters* **114**, 200501 (2015).
- [16] Z.-H. Ding, J.-M. Cui, Y.-F. Huang, C.-F. Li, T. Tu, and G.-C. Guo, *Physical Review Applied* **12**, 014038 (2019).
- [17] P. Qian, X. Lin, F. Zhou, R. Ye, Y. Ji, B. Chen, G. Xie, and N. Xu, *Applied Physics Letters* **118**, 084001 (2021).
- [18] A. Hentschel and B. C. Sanders, *Physical review letters* **104**, 063603 (2010).
- [19] A. Lumino, E. Polino, A. S. Rab, G. Milani, N. Spagnolo, N. Wiebe, and F. Sciarrino, *Physical Review Applied* **10**, 044033 (2018).
- [20] M. Krenn, M. Malik, R. Fickler, R. Lapkiewicz, and A. Zeilinger, *Physical review letters* **116**, 090405 (2016).
- [21] A. A. Melnikov, H. P. Nautrup, M. Krenn, V. Dunjko, M. Tiersch, A. Zeilinger, and H. J. Briegel, *Proceedings of the National Academy of Sciences* **115**, 1221 (2018).
- [22] G. E. Hinton and R. R. Salakhutdinov, *science* **313**, 504 (2006).
- [23] G. Carleo and M. Troyer, *Science* **355**, 602 (2017).
- [24] A. S. Weigend, *Time series prediction: forecasting the future and understanding the past* (Routledge, 2018).
- [25] J. R. Maze, P. L. Stanwix, J. S. Hodges, S. Hong, J. M. Taylor, P. Cappellaro, L. Jiang, M. V. Dutt, E. Togan, A. S. Zibrov, A. Yacoby, R. L. Walsworth, and M. D. Lukin, *Nature* **455**, 644 (2008).
- [26] G. Balasubramanian, I. Y. Chan, R. Kolesov, M. Al-Hmoud, J. Tisler, C. Shin, C. Kim, A. Wojcik, P. R. Hemmer, A. Krueger, T. Hanke, A. Leitenstorfer, R. Bratschitsch, F. Jelezko, and J. Wrachtrup, *Nature* **455**, 648 (2008).

- [27] M. S. Grinolds, S. Hong, P. Maletinsky, L. Luan, M. D. Lukin, R. L. Walsworth, and A. Yacoby, *Nature Physics* **9**, 215 (2013).
- [28] G. Waldherr, J. Beck, P. Neumann, R. Said, M. Nitsche, M. Markham, D. Twitchen, J. Twamley, F. Jelezko, and J. Wrachtrup, *Nature nanotechnology* **7**, 105 (2012).
- [29] T. Unden, P. Balasubramanian, D. Louzon, Y. Vinkler, M. Plenio, M. Markham, D. Twitchen, A. Stacey, I. Lovchinsky, A. Sushkov, M. Lukin, A. Retzker, B. Naydenov, L. McGuinness, and F. Jelezko, *Physical Review Letters* **116**, 230502 (2016).
- [30] I. Jakobi, P. Neumann, Y. Wang, D. B. R. Dasari, F. El Hallak, M. A. Bashir, M. Markham, A. Edmonds, D. Twitchen, and J. Wrachtrup, *Nature nanotechnology* **12**, 67 (2017).
- [31] F. Dolde, H. Fedder, M. W. Doherty, T. Nöbauer, F. Rempp, G. Balasubramanian, T. Wolf, F. Reinhard, L. C. L. Hollenberg, F. Jelezko, and J. Wrachtrup, *Nature Physics* **7**, 459 (2011).
- [32] R. Li, F. Kong, P. Zhao, Z. Cheng, Z. Qin, M. Wang, Q. Zhang, P. Wang, Y. Wang, F. Shi, and J. Du, *Physical Review Letters* **124**, 247701 (2020).
- [33] G. Kucsko, P. C. Maurer, N. Y. Yao, M. Kubo, H. J. Noh, P. K. Lo, H. Park, and M. D. Lukin, *Nature* **500**, 54 (2013).
- [34] D. M. Toyli, C. F. de las Casas, D. J. Christle, V. V. Dobrovitski, and D. D. Awschalom, *Proc Natl Acad Sci U S A* **110**, 8417 (2013).
- [35] S. Schmitt, T. Gefen, F. M. Stárner, T. Unden, G. Wolff, C. Müller, J. Scheuer, B. Naydenov, M. Markham, S. Pezzagna, J. Meijer, I. Schwarz, M. Plenio, A. Retzker, L. P. McGuinness, and F. Jelezko, *Science* **356**, 832 (2017).
- [36] T. Staudacher, F. Shi, S. Pezzagna, J. Meijer, J. Du, C. A. Meriles, F. Reinhard, and J. Wrachtrup, *Science* **339**, 561 (2013).
- [37] H. Mamin, M. Kim, M. Sherwood, C. Rettner, K. Ohno, D. Awschalom, and D. Rugar, *Science* **339**, 557 (2013).
- [38] F. Shi, F. Kong, P. Zhao, X. Zhang, M. Chen, S. Chen, Q. Zhang, M. Wang, X. Ye, and Z. Wang, *Nature methods* **15**, 697 (2018).
- [39] N. Aslam, M. Pfender, P. Neumann, R. Reuter, A. Zappe, F. F. de Oliveira, A. Denisenko, H. Sumiya, S. Onoda, J. Isoya, and J. Wrachtrup, *Science* **357**, 67 (2017).
- [40] L. Childress, M. G. Dutt, J. Taylor, A. Zibrov, F. Jelezko, J. Wrachtrup, P. Hemmer, and M. Lukin, *Science* **314**, 281 (2006).
- [41] M. V. G. Dutt, L. Childress, L. Jiang, E. Togan, J. Maze, F. Jelezko, A. S. Zibrov, P. R. Hemmer, and M. D. Lukin, *Science* **316**, 1312 (2007).
- [42] G. D. Fuchs, G. Burkard, P. V. Klimov, and D. D. Awschalom, *Nature Physics* **7**, 789 (2011).
- [43] Q. Zhang, Y. Guo, W. Ji, M. Wang, J. Yin, F. Kong, Y. Lin, C. Yin, F. Shi, Y. Wang, and J. Du, *Nature Communications* **12**, 1529 (2021).
- [44] F. Shi, X. Rong, N. Xu, Y. Wang, J. Wu, B. Chong, X. Peng, J. Knipfert, R.-S. Schoenfeld, W. Harneit, M. Feng, and J. Du, *Physical Review Letters* **105**, 040504 (2010).
- [45] C. Zu, W.-B. Wang, L. He, W.-G. Zhang, C.-Y. Dai, F. Wang, and L.-M. Duan, *Nature* **514**, 72 (2014).
- [46] T. van der Sar, Z. H. Wang, M. S. Blok, H. Bernien, T. H. Taminiau, D. M. Toyli, D. A. Lidar, D. D. Awschalom, R. Hanson, and V. V. Dobrovitski, *Nature* **484**, 82 (2012).
- [47] T. H. Taminiau, J. Cramer, T. van der Sar, V. V. Dobrovitski, and R. Hanson, *Nature nanotechnology* **9**, 171 (2014).
- [48] K. Xu, T. Xie, Z. Li, X. Xu, M. Wang, X. Ye, F. Kong, J. Geng, C. Duan, F. Shi, and J. Du, *Physical review letters* **118**, 130504 (2017).
- [49] J. Cai, A. Retzker, F. Jelezko, and M. B. Plenio, *Nature Physics* **9**, 168 (2013).
- [50] W. Ji, L. Zhang, M. Wang, L. Zhang, Y. Guo, Z. Chai, X. Rong, F. Shi, X.-J. Liu, Y. Wang, and J. Du, *Physical Review Letters* **125**, 020504 (2020).
- [51] S. Yang, Y. Wang, D. D. B. Rao, T. H. Tran, A. S. Momenzadeh, M. Markham, D. J. Twitchen, P. Wang, W. Yang, R. Stárner, P. Neumann, H. Kosaka, and J. Wrachtrup, *Nature Photonics* **10**, 507 (2016).
- [52] A. Reiserer, N. Kalb, M. S. Blok, K. J. van Bemmel, T. H. Taminiau, R. Hanson, D. J. Twitchen, and M. Markham, *Physical Review X* **6**, 021040 (2016).
- [53] N. Kalb, A. A. Reiserer, P. C. Humphreys, J. J. W. Bakermans, S. J. Kamerling, N. H. Nickerson, S. C. Benjamin, D. J. Twitchen, M. Markham, and R. Hanson, *Science* **356**, 928 (2017).
- [54] P. C. Humphreys, N. Kalb, J. P. J. Morits, R. N. Schouten, R. F. L. Vermeulen, D. J. Twitchen, M. Markham, and R. Hanson, *Nature* **558**, 268 (2018).
- [55] M. Pompili, S. L. N. Hermans, S. Baier, H. K. C. Beukers, P. C. Humphreys, R. N. Schouten, R. F. L. Vermeulen, M. J. Tiggelman, L. d. S. Martins, B. Dirkse, S. Wehner, and R. Hanson, *Science* **372**, 259 (2021).
- [56] See Supplemental Online Materials for details of single-spin lock-in detection, numerical simulation and additional XY8 spectrum of NV2.
- [57] S. Hochreiter and J. Schmidhuber, *Neural computation* **9**, 1735 (1997).
- [58] M. Hirose and P. Cappellaro, *Nature* **532**, 77 (2016).
- [59] M. Pfender, N. Aslam, H. Sumiya, S. Onoda, P. Neumann, J. Isoya, C. A. Meriles, and J. Wrachtrup, *Nature Communications* **8**, 834 (2017).
- [60] J. R. Johansson, P. D. Nation, and F. Nori, *Computer Physics Communications* **183**, 1760 (2012).
- [61] J. D. Hunter, *Computing in science and engineering* **9**, 90 (2007).
- [62] A. Paszke, S. Gross, F. Massa, A. Lerer, J. Bradbury, G. Chanan, T. Killeen, Z. Lin, N. Gimelshein, and L. Antiga, *Advances in neural information processing systems* **32**, 8026 (2019).